

PAPER • OPEN ACCESS

# Contact resistance and mobility in back-gate graphene transistors

To cite this article: Francesca Urban *et al* 2020 *Nano Express* 1 010001

View the [article online](#) for updates and enhancements.

## Recent citations

- [Welcome to Nano Express](#)  
Antonio Di Bartolomeo



## PAPER

## Contact resistance and mobility in back-gate graphene transistors

## OPEN ACCESS

## RECEIVED

6 December 2019

## REVISED

21 January 2020

## ACCEPTED FOR PUBLICATION

27 January 2020

## PUBLISHED

16 March 2020

Original content from this work may be used under the terms of the [Creative Commons Attribution 4.0 licence](#).

Any further distribution of this work must maintain attribution to the author(s) and the title of the work, journal citation and DOI.



Francesca Urban<sup>1,4</sup>, Grzegorz Lupina<sup>2</sup>, Alessandro Grillo<sup>1</sup>, Nadia Martucciello<sup>3</sup> and Antonio Di Bartolomeo<sup>1,4</sup>

<sup>1</sup> Physics Department, University of Salerno, INFN - Gruppo collegato di Salerno, and CNR-Spin, 84084 Fisciano, Salerno, Italy

<sup>2</sup> IHP-Microelectronics, Im Technologiepark 25, 15236 Frankfurt (Oder); currently with Infineon Technologies Austria, Germany

<sup>3</sup> CNR-Spin, 84084 Fisciano, Salerno, Italy

<sup>4</sup> Authors to whom any correspondence should be addressed.

E-mail: [furban@unisa.it](mailto:furban@unisa.it) and [adibartolomeo@unisa.it](mailto:adibartolomeo@unisa.it)

**Keywords:** graphene, contact resistance, mobility, temperature dependence, TLM structures, Y-function method, field effect transistors

## Abstract

The metal-graphene contact resistance is one of the major limiting factors toward the technological exploitation of graphene in electronic devices and sensors. High contact resistance can be detrimental to device performance and spoil the intrinsic great properties of graphene. In this paper, we fabricate back-gate graphene field-effect transistors with different geometries to study the contact and channel resistance as well as the carrier mobility as a function of gate voltage and temperature. We apply the transfer length method and the  $\gamma$ -function method showing that the two approaches can complement each other to evaluate the contact resistance and prevent artifacts in the estimation of carrier mobility dependence on the gate-voltage. We find that the gate voltage modulates both the contact and the channel resistance in a similar way but does not change the carrier mobility. We also show that raising the temperature lowers the carrier mobility, has a negligible effect on the contact resistance, and can induce a transition from a semiconducting to a metallic behavior of the graphene sheet resistance, depending on the applied gate voltage. Finally, we show that eliminating the detrimental effects of the contact resistance on the transistor channel current almost doubles the carrier field-effect mobility and that a competitive contact resistance as low as  $700 \Omega \cdot \mu\text{m}$  can be achieved by the zig-zag shaping of the Ni contact.

## 1. Introduction

The isolation of graphene [1–3] in 2004 and, later on, of h-BN [4], phosphorene [5], MoS<sub>2</sub> [6–14], WSe<sub>2</sub> [15–17], PdSe<sub>2</sub> [18, 19], PtSe<sub>2</sub> [20, 21] etc, has strongly attracted the interest of the material science community to the world of two-dimensional (2D) materials.

Graphene, the two-dimensional layer of carbon atoms arranged in a honeycomb lattice, is still one of the most studied 2D systems for the unmatched electron mobility, the remarkable current capability and thermal conduction, the relatively high optical absorption coefficient, the mechanical strength as well as the easy and low cost fabrication [22–27].

Graphene is commonly produced by exfoliation from graphite [28, 29], epitaxial growth on SiC [30] or chemical vapor deposition (CVD) [31, 32]. In particular, CVD produces uniform and large-scale graphene flakes of high-quality and is compatible with the silicon technology; therefore, it has been largely exploited to realize new electronic devices such as diodes [33–36], transistors [37–39], field emitters [40, 41], chemical-biological sensors [42, 43], optoelectronic systems [44], photodetectors [45–50] and solar cells [51].

Due to its gapless band-structure, with the valence and conduction bands touching each other at the so-called Dirac points, graphene originates ambipolar field-effect transistors with V-shaped transfer characteristics, dominated by a p-branch at negative and n-type conduction at positive gate voltage [52]. The ambipolar conduction can be an important feature for complementary logic applications; however, the limited on/off ratio

caused by the absence of intrinsic bandgap is a significant obstacle and requires delicate material engineering for real applications [53–55].

Despite the several doping techniques available to tune the graphene conductivity and boost the performance of graphene transistors, a major problem remains the suppression of device on-current caused by the graphene/contact resistance [56]. Indeed, ohmic and low resistance contacts are important figures of merit for high frequency devices and the realization of stable and low-resistance contacts is still under intensive study [57–61]. The variation of the contact resistance,  $R_C$ , is attributed to many different causes, related to graphene growth and number of layers, metal type and deposition process, quality of the metal/graphene/interface, measurement conditions, etc.

Conventional ohmic contacts between graphene and various metals exhibit rather large contact resistance ranging from few hundreds to thousands  $\Omega \cdot \mu\text{m}$ . Studies have been conducted on various types of metal/graphene interfaces showing that the best contact resistances can be achieved with Ni and Cu contacts yielding  $R_C$  as low as  $\sim 300 \Omega$  [62–65]. Although the choice of the metal type is an important ingredient for good quality contacts, recent researches have developed special techniques for the reduction of the contact resistance. The most successful strategies have been the modification of the contact area to increase charge injection through the graphene edges and the graphene etching under the contacts to favor the formation of dangling carbon-to-metal bonds. Contact resistances down to  $100 \Omega \cdot \mu\text{m}$  have been obtained in this way [63, 65–67]. Anzi *et al* [67] report that the under-contact graphene etching reduces the contact resistance both for Au and Ni/Au contacts. Smith *et al* [63] demonstrate a contact resistance dependence on the number of graphene cuts under the contacts. Similarly, Lisker *et al* [57] optimize the metal/graphene interface by incrementing the contact perimeter. A low contact resistance enables the study of intrinsic graphene properties and increases the performance of graphene devices. As the matter of fact, the contact resistance can be tuned by the application of a gate voltage ( $V_{gs}$ ), which modulates the carrier concentration of the graphene channel. In this scenario, the contact resistance becomes larger in correspondence of the Dirac points, where the graphene conductivity is suppressed [68, 69].

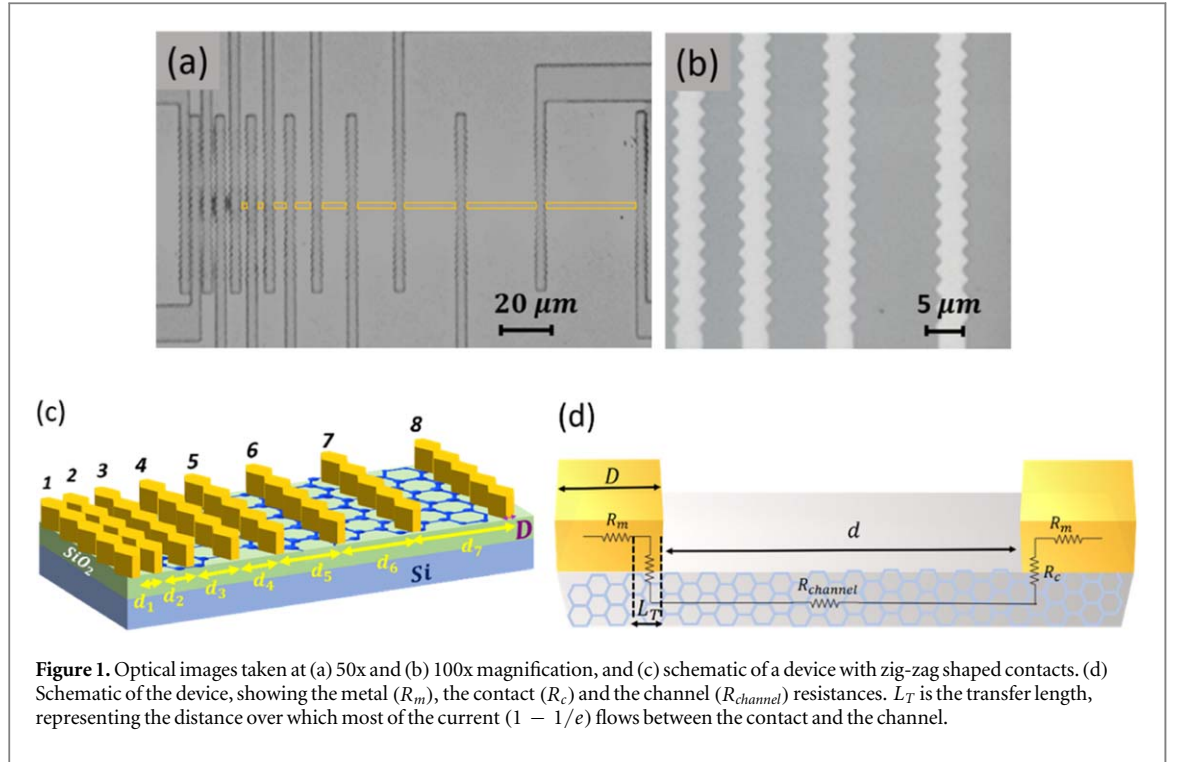
The temperature dependence of  $R_C$  in graphene devices is still a controversial topic. A conspicuous number of studies report discrepant results evidencing either a negligible dependence of  $R_C$  on T or strong changes of contact resistance with temperature [70–72].

In this work, we investigate the effect of back-gate voltage and temperature on the contact and channel resistance and on the carrier mobility in graphene field-effect transistors with Ni contacts. We fabricate back-gate devices with multiple leads which we analyze by both the transfer length method (TLM) [73–77] and the Y-function method [78–80]. The complementary application of the two methods leads to a more robust estimation of the contact resistance and of the gate-voltage dependence of the carrier mobility. We show that the gate voltage modulates the contact and the channel resistance in a similar way but has negligible effect on the carrier mobility. We also find that the field effect mobility decreases with raising the temperature, which does not affect the contact resistance, but can induce a transition from a semiconducting to a metallic behavior in the channel resistance, depending on the gate voltage. Finally, we show that eliminating the detrimental effect of the contact resistance can result in more than 80% increase of the field effect mobility.

## 2. Materials and methods

Graphene synthesis has been performed on 200 mm Ge/Si substrates using Aixtron's Black Magic BM300T CVD tool. The synthesis was carried out at the deposition temperatures of 885 °C using  $\text{CH}_4$  as source of carbon and Ar/ $\text{H}_2$  mixture as carrier gas, at 700 mbar for 60 min Raman and micro-Raman mapping confirmed that the optimized fabrication process led to high quality, defect-free, and uniform graphene film over the whole wafer [57, 81]. The so-obtained graphene was then transferred on p-type doped Si ( $5 - 20 \Omega \cdot \text{cm}$ ) capped with 100 nm  $\text{SiO}_2$  layer, patterned in long stripes by electron beam lithography (EBL) and dry etching, and finally covered by PMMA to prevent damages. Ni metal contacts were sputtered using a 50 W low-power process after keeping the sample degassing in vacuum at pressure  $< 10^{-8}$  mbar for 24 h. An annealing in 1:2 mixture of hydrogen and argon at 580 °C for 30 min was applied to further reduce the specific contact resistivity. The devices consist of patterned graphene stripes contacted with several parallel leads, at gradually increasing distances ( $d_i$ ). Structures with diverse combinations of the contact size, distance and/or shape, were fabricated and analyzed as well, with an example reported in figures 1(a), (b).

Measurements at different temperatures were performed using a Janis probe station equipped with four metallic nanotips connected to the source-measurement units of a Keithley 4200 SCS (Tektronix Inc.), at pressure of  $\sim 0.8$  mbar. The metal contacts were used as the drain and source electrodes while the Si/ $\text{SiO}_2$  substrate as the back gate and the gate dielectric, respectively.



The schematic of figure 1(d) shows that the total resistance,  $R_T$ , obtained from the  $I_{ds} - V_{ds}$  (drain-to-source current versus drain-to-source voltage) curves measured in a two-probe configuration between two given contacts, includes the contributions of the metal resistance,  $R_m$ , the contact resistance,  $R_C$ , i.e. the resistance at the 3D-metal/2D-graphene interface, and the channel resistance,  $R_{channel}$ :

$$R_T = R_{channel} + 2R_m + 2R_C \quad (1)$$

The channel resistance can be written as

$$R_{channel} = R_{sheet} \frac{d}{W} \quad (2)$$

where  $R_{sheet}$  is the graphene sheet resistance in  $\Omega/sq$  ( $sq = \text{square}$ ),  $W$  the width of the graphene stripe and  $d$  the distance between the two chosen contacts. We can express the contact resistance in terms of the transfer length,  $L_T$ , that represents the distance over which most of the current ( $1 - 1/e$ ) flows between the contact and the channel:  $R_C = R_{sheet} \frac{L_T}{W}$  [82]. Therefore, neglecting  $R_m$  (order of magnitude lower than  $R_C$  and  $R_{channel}$ ), it results

$$R_T = R_{sheet} \frac{d}{W} + 2R_C = \frac{R_{sheet}}{W} (d + 2L_T) \quad (3)$$

Equation (3) is used to estimate  $R_{sheet}$  and  $R_C$  from the straight-line fitting of a  $R_T$  vs  $d$  plot (TLM plot). The intercept of the straight-line with the horizontal axis ( $-2L_T$ ) provides the transfer length. If  $L_T$  is small compared to the size  $D$  of the contact, the current flows mostly through the edge of the contact (current crowding effect) and only the contact edge influences the carrier injection and the conduction in the graphene channel. In this scenario, there are only two possibilities to reduce the contact resistance: etching the graphene under the contact to increase the contact edges or increasing the perimeter of the edge, for instance using zig-zag shaped edges.

For two-probe configuration measurements, an alternative approach to estimate the contact resistance is the so-called Y-function method (YFM). The method includes the contact resistance in the expression of the transistor current  $I_{ds}$  as a function of  $V_{ds}$  and  $V_{gs}$  (the gate-to-source voltage) [79, 83]:

$$I_{ds} = \frac{\frac{W}{L} \mu C_{ox} V_{ds} (V_{gs} - V_{Dirac})}{1 + \frac{W}{L} \mu C_{ox} R_C (V_{gs} - V_{Dirac})} \quad (4)$$

where  $C_{ox}$  is the SiO<sub>2</sub> capacitance ( $C_{ox} = 33 \text{ nFcm}^{-2}$  for 100 nm SiO<sub>2</sub>),  $\mu$  is the field-effect mobility and  $V_{Dirac}$  is the gate voltage corresponding to the Dirac point, i.e. to the minimum of the  $I_{ds} - V_{gs}$  characteristic of the graphene transistor.

The  $V_{gs}$  derivative of equation (4) represents the transconductance

$$g_m = \frac{dI_{ds}}{dV_{gs}} = \frac{\frac{W}{L}\mu C_{ox} V_{ds}}{\left[1 + \frac{W}{L}\mu C_{ox} R_C (V_{gs} - V_{Dirac})\right]^2} \quad (5)$$

and the ratio

$$\frac{I_{ds}}{\sqrt{g_m}} = \sqrt{\frac{W}{L}\mu C_{ox} V_{ds} (V_{gs} - V_{Dirac})} = Y \quad (6)$$

is the so-called Y-function. Y results independent of  $R_C$ , while  $g_m^{-1/2}$  depends linearly on  $(V_{gs} - V_{Dirac})$  with angular coefficient proportional to the contact resistance. Thus, the plots of  $I_{ds}g_m^{-1/2}$  and  $g_m^{-1/2}$  versus  $(V_{gs} - V_{Dirac})$  can be exploited to obtain the mobility  $\mu$  (which is not affected by the contact resistance) and the contact resistance  $R_C$ , respectively.

Finally, taking the derivative of the Y-function in equation (6) with respect to  $V_{gs} - V_{Dirac}$ , we obtain the mobility unaffected by the contact resistance, which should be independent of  $V_{gs} - V_{Dirac}$ :

$$\mu = \left[ \frac{dY}{d(V_{gs} - V_{Dirac})} \right]^2 \frac{L}{WC_{ox} V_{ds}} \quad (7)$$

### 3. Results and discussion

A two-probe configuration is adopted to measure the transfer ( $I_{ds} - V_{gs}$  curve at given  $V_{ds}$ ) and output ( $I_{ds} - V_{ds}$  curves at selected  $V_{gs}$ ) characteristics for different contact combinations. In figure 2, we report an example of such measurements for the 2  $\mu\text{m}$  wide and 1  $\mu\text{m}$  long graphene channel contacted with Ni leads of size  $D \sim 3 \mu\text{m}$  and zig-zag shaped edges (see figures 1(a), (b) and the schematic of the device figure 1(c)).

The transfer characteristic (figure 2(a)) displays an asymmetric ambipolar behavior with a dominant hole branch and a current minimum (Dirac point) slightly above  $V_{gs} = 0 \text{ V}$ . The different slope of the two branches corresponds to the hole mobility ( $\sim 150 \text{ cm}^2\text{V}^{-1}\text{s}^{-1}$ ) higher than the electron one ( $\sim 100 \text{ cm}^2\text{V}^{-1}\text{s}^{-1}$ ), while the slight shift of the Dirac point to positive  $V_{gs}$  indicates a low p-type carrier concentration due to adsorbates and process residues such as PMMA, not removed by the 1 mbar vacuum and 400 K annealing [59, 84]. The hole-electron asymmetry is due to both unbalanced carrier injection from metal contacts and graphene interaction with the SiO<sub>2</sub> dielectric [84–89]. The interaction with SiO<sub>2</sub> is also the main cause of the hysteresis which appears when the gate voltage is swept back and forth [88–90]. The low mobility is also attributed to the fabrication process which needs further optimization. Figure 2(b) shows a linear  $I_{ds} - V_{ds}$  behavior confirming the ohmic nature of the Ni/graphene contacts in the investigated voltage range. We intentionally limited the analysis to the triode region, as the achievement of a saturation regime would require operating the transistor at high drain bias and power dissipation, which would make the local temperature out of control.

Figure 3(a) shows the total resistance  $R_T$  measured between multiple couples of leads of the TLM structure, at room temperature and under different gate biases, ranging from  $-40 \text{ V}$  to  $40 \text{ V}$ . The TLM curves display the linear behavior predicted by equation (3) and are used to extract  $R_C$  and  $R_{sheet}$  as a function of the gate voltage  $V_{gs}$  (figure 3(b)). Both parameters exhibit a non-monotonic trend with maximum values ( $R_C \sim 2.5 \text{ k}\Omega$  and  $R_{sheet} \sim 14 \text{ k}\Omega/\text{sq}$ ) corresponding to the Dirac point ( $V_{Dirac} \sim 0 \text{ V}$ ), and a decrease when the back-gate dopes the graphene by attracting electrons or holes in the channel. We highlight that figure 3(b) demonstrates how the gate voltage affects the graphene layer not only in the channel region but also under the contacts, as previously reported [91].

$L_T$  extracted from the  $R_T$  versus  $d$  plot ranges between 300 nm and 500 nm, smaller the 3  $\mu\text{m}$  contact size, thereby confirming that the device works under the aforementioned current crowding regime.

Remarkably, comparison with a similar device contacted by straight contacts, i.e. no zig-zag edges, measured in the same conditions, exhibits  $\sim 400\%$  higher contact resistance ( $\sim 3.5 \text{ k}\Omega \cdot \mu\text{m}$  versus  $\sim 700 \Omega \cdot \mu\text{m}$  at  $V_{gs} = -40 \text{ V}$ ), confirming the importance of increasing the length of the contact perimeter.

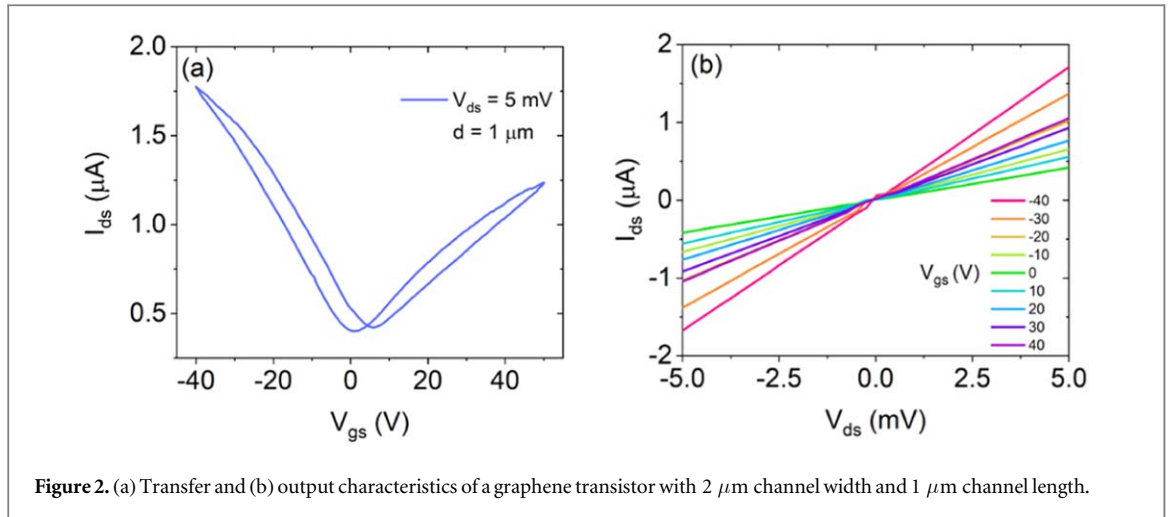


**Figure 2.** (a) Transfer and (b) output characteristics of a graphene transistor with 2  $\mu\text{m}$  channel width and 1  $\mu\text{m}$  channel length.

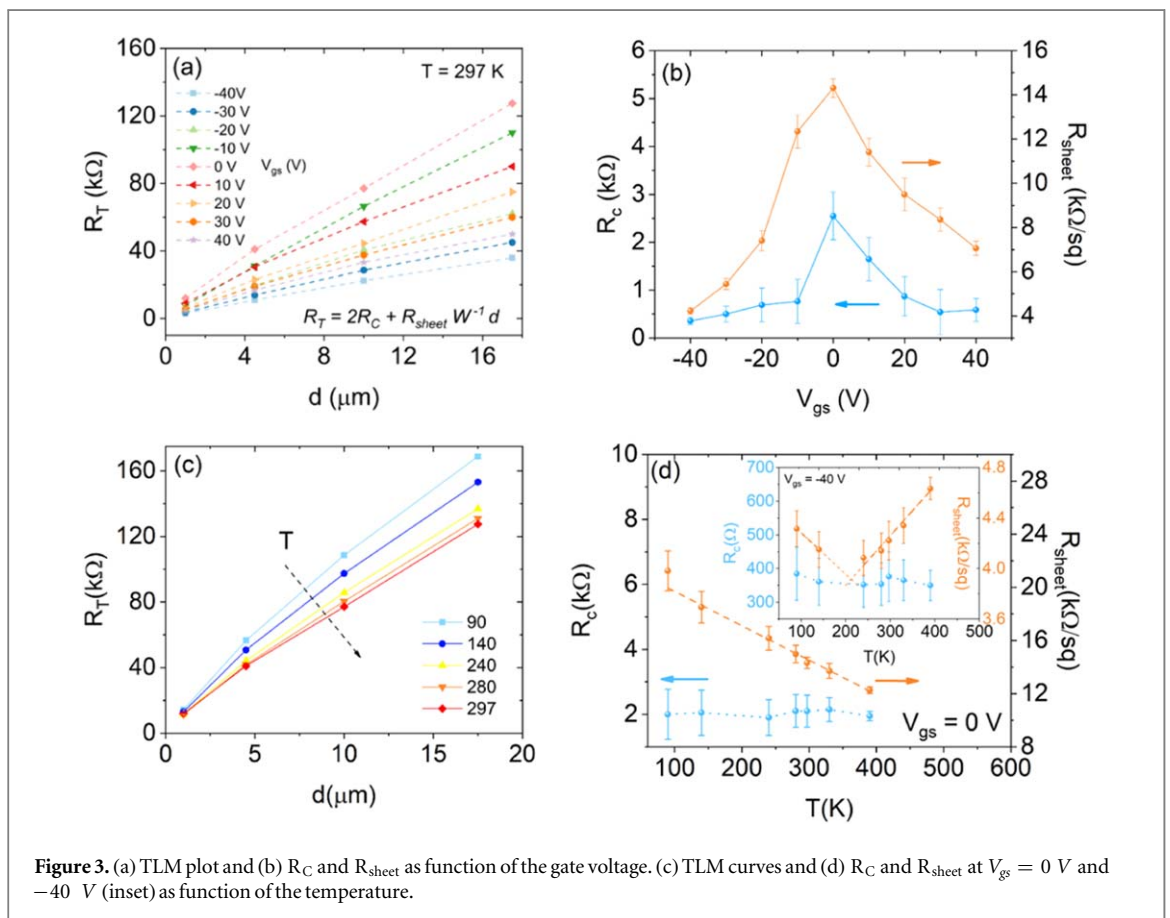
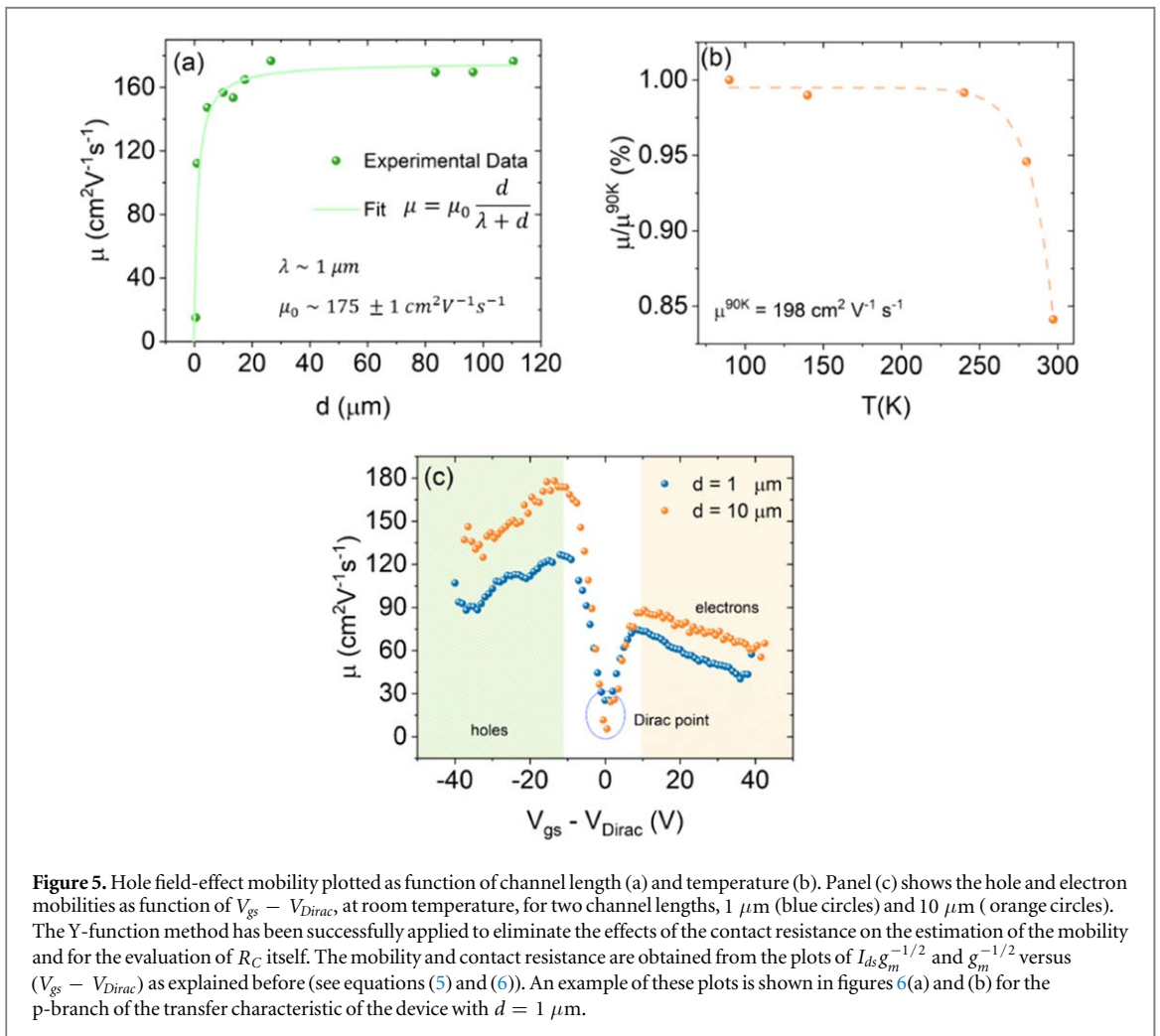
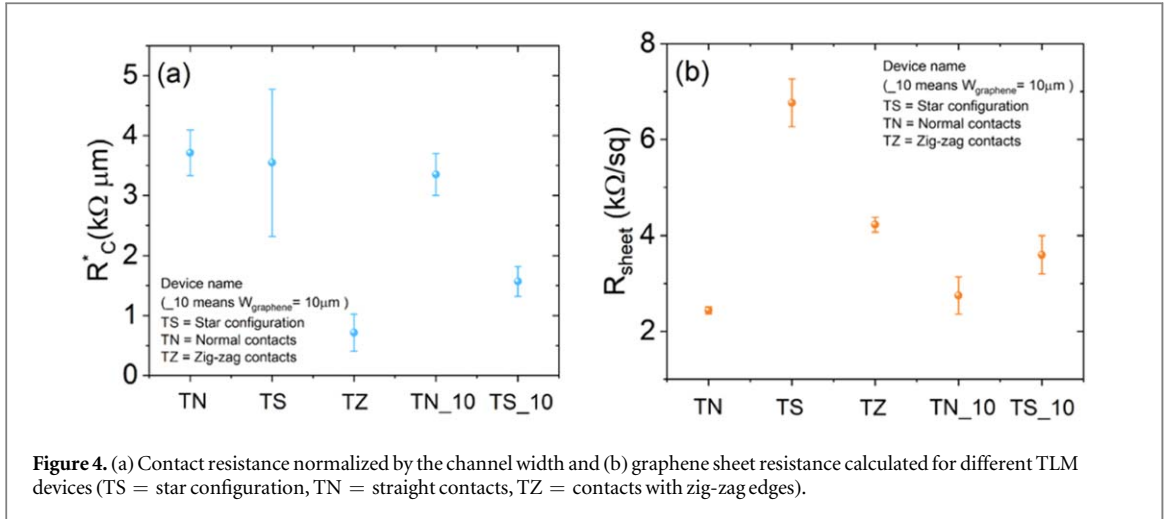


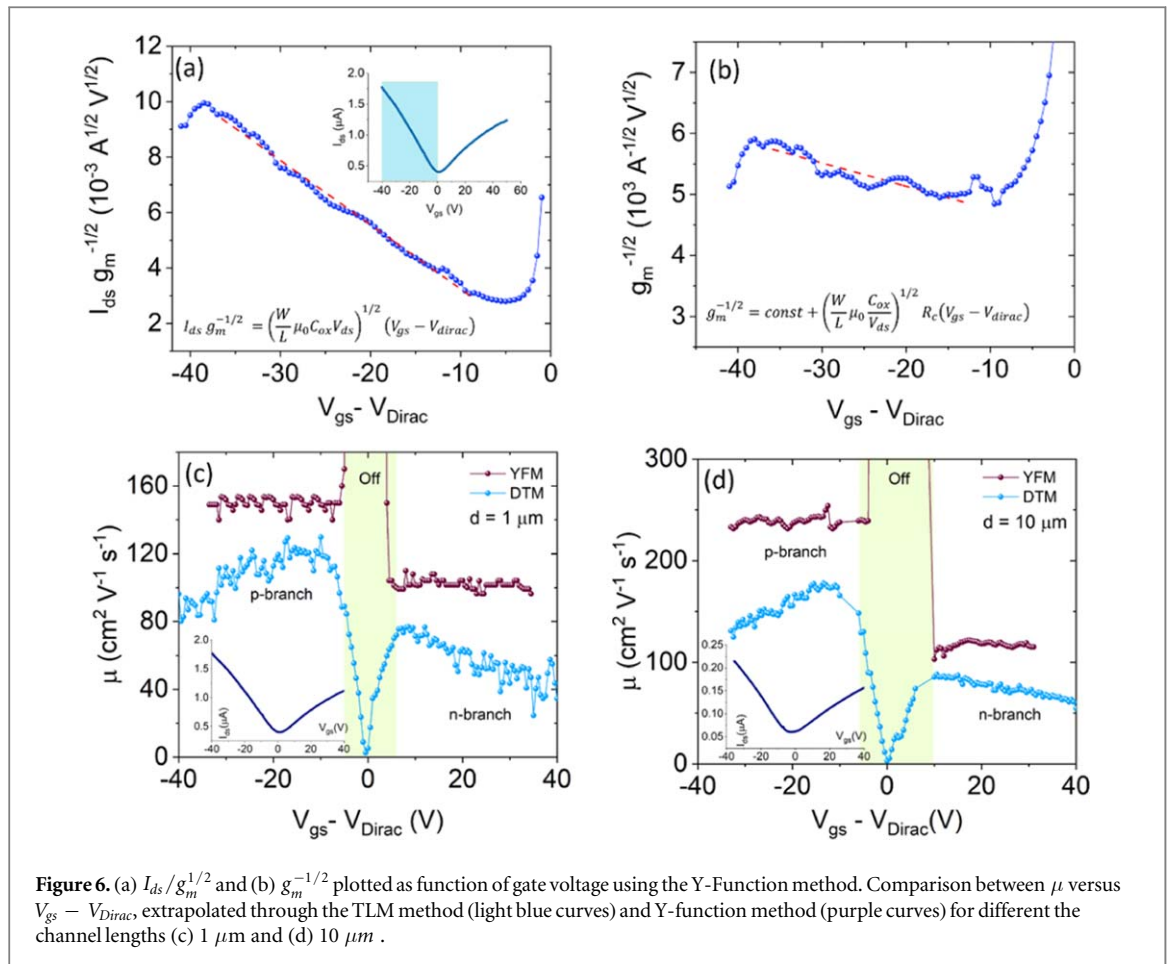
**Figure 3.** (a) TLM plot and (b)  $R_C$  and  $R_{\text{sheet}}$  as function of the gate voltage. (c) TLM curves and (d)  $R_C$  and  $R_{\text{sheet}}$  at  $V_{\text{gs}} = 0 \text{ V}$  and  $-40 \text{ V}$  (inset) as function of the temperature.

Similar measurements were performed as a function of the temperature,  $T$ , in the range 90 K to 400 K. The linear behavior of the  $R_T$  vs  $d$  curves is preserved when the temperature is changed (figure 3(c)) but their slope decreases with increasing  $T$ . Figure 3(d) reports the temperature dependence of  $R_C$  and  $R_{\text{sheet}}$  evaluated at  $V_{\text{gs}} = 0 \text{ V}$ .  $R_C$  remains constant over the 90–400 K temperature range while the graphene sheet resistance decreases, changing linearly from  $\sim 22 \text{ k}\Omega/\text{sq}$  at 90 K to  $\sim 12 \text{ k}\Omega/\text{sq}$  at 400 K with slope  $dR_{\text{sheet}}/dT \sim -15 \text{ }\Omega/\text{K}$ . The independence of  $R_C$  on the temperature is confirmed also when  $R_C$  is evaluated at  $V_{\text{gs}} = -40 \text{ V}$ , as shown in the inset of figure 3(d). Conversely, a new feature appears in the temperature behavior of  $R_{\text{sheet}}$  at  $V_{\text{gs}} = -40 \text{ V}$ : the sheet resistance decreases until the temperature reaches  $\sim 200 \text{ K}$  and raises for  $T \geq 200 \text{ K}$  up to  $\sim 4.8 \text{ }\Omega/\text{sq}$  at  $T = 400 \text{ K}$ . Otherwise stated, a transition from a semiconducting to a metallic behavior occurs in graphene around  $T \sim 200 \text{ K}$ , consistently with what has been observed before [92–95]. Similar TLM analyses have been conducted on devices of the same chip with graphene channel 2  $\mu\text{m}$  or 10  $\mu\text{m}$  wide or with different layout. The estimated contact resistance, normalized by the channel width,  $R_C^* = R_C W$ , and sheet resistances are summarized in figure 4, showing a mean  $R_C^*$  value of  $\sim 2 \text{ k}\Omega \cdot \mu\text{m}$  and



$R_{sheet} \sim 4 \text{ k}\Omega/\text{sq}$ . We note that, owed to the zig-zag geometry, the TZ structure in figure 4 (which is the previously analyzed one), shows a normalized contact resistance as low as  $R_C^* \sim 700 \Omega \cdot \mu\text{m}$  at  $V_{gs} = -40 \text{ V}$  within the range of the good quality contacts typically reported in the literature [63, 65–67]. Considering that the device-to-device fluctuations across the wafer are less than 30% [54], the improvement of the zig-zag geometry is highly significant. The differences in the sheet resistance shown in figure 4(b) can be attributed to local variations of the transferred graphene foil and different damage induced by the fabrication process.

We further exploited the TLM measurements to study the dependence of the field-effect mobility,  $\mu$ , on the channel length  $d$  and the temperature. The mobility was estimated from the slope  $\frac{dI_{ds}}{dV_{gs}}$  of the linear part of the



transfer characteristics as

$$\mu = \frac{d}{WC_{ox} V_{ds}} \frac{dI_{ds}}{dV_{gs}} \quad (8)$$

Figure 5(a) shows the hole mobility as function of channel length, an increase of  $\mu$  with  $d$  appears for small  $d$  with a further saturation at larger channel lengths.. Such a behavior can be expressed as  $\mu = \mu_0 \frac{d}{d + \lambda}$ , where  $\mu_0$  is the saturated mobility and  $\lambda$  the mean free path [96]. From the fit of the experimental data, we obtain  $\lambda \sim 1 \mu\text{m}$  and  $\mu_0 \sim 175 \text{ cm}^2 \text{V}^{-1} \text{s}^{-1}$ . The saturation at channel length  $d \gg \lambda$  corresponds to the establishment of a diffusive transport regime, while the mobility degradation at lower  $d$  ( $d \leq \lambda$ ) is an artifact due to the application of equation (8) in a regime where the transport becomes quasi-ballistic or ballistic [96, 97]. The influence of the temperature on the mobility, for the chosen device with  $d = 110 \mu\text{m}$ , is shown in figure 5(b), which indicates that most of the mobility degradation occurs for  $T > 250 \text{ K}$  ( $\sim 15\%$  from its value at  $90 \text{ K}$ ,  $\mu_{90\text{K}} \sim 195 \text{ cm}^2 \text{V}^{-1} \text{s}^{-1}$ ). This behavior can be understood considering that phonon scattering in graphene becomes relevant only at higher temperatures [98–100].

The electron/hole mobilities evaluated from the numerical derivative of the  $I_{ds} - V_{gs}$  curves according to equation (8), are plotted in figure 5(c) as function of  $V_{gs} - V_{Dirac}$  (gate overdrive) for two channel lengths ( $1$  and  $10 \mu\text{m}$ , respectively). The mobilities show a minimum at the Dirac point, reach a maximum for increasing overdrive and decrease smoothly for  $|V_{gs} - V_{Dirac}| > 10 \text{ V}$ . The contact resistance, whose effect on the mobility is not eliminated in this type of analysis, could cause this decrease of  $\mu$  with gate overdrive. To confirm such a hypothesis and obtain a more accurate  $\mu$  versus  $V_{gs}$  behavior, we considered the Y-function method as complementary approach to the TLM analysis.

From figure 6(a), we obtained a field effect mobility  $\mu \sim 160 \text{ cm}^2 \text{V}^{-1} \text{s}^{-1}$ , which together with the data in figure 6(b) yields  $R_C = 310 \Omega$  (or  $R_C^* = 700 \Omega \cdot \mu\text{m}$ ). These values are consistent with the results from the TLM analysis.

The plots of the mobility versus  $V_{gs} - V_{Dirac}$  (figures 6(c) and (d) for  $1 \mu\text{m}$  and  $10 \mu\text{m}$  channel lengths, respectively) show that  $\mu$  is unaffected by  $R_C$  and is independent of the gate overdrive. The elimination of the contact resistance effect by the YFM confirms that gate dependence of the field-effect mobility is only an artifact of the TLM method.

We also note from figures 6(c) and (d) that removing  $R_C$  results in significantly higher mobility, with over 80% increase.

## 4. Conclusions

In conclusion, we have fabricated and analyzed Ni-contacted graphene FETs and studied the back-gate and temperature dependence of the contact and channel resistance. We have measured devices with different geometrical structures and achieved competitive contact resistances using zig-zag shaped Ni contacts, also confirming the importance of contact geometry in the metal/graphene contact resistance.

We have found that the gate voltage modulates the contact and the channel resistance in a similar way but does not change the carrier mobility. We have also shown that raising the temperature decreases the carrier mobility, has a negligible effect on the contact resistance and can change the initial semiconducting behavior of the channel resistance into a metallic one, depending on the gate voltage. We used two complementary methods, namely the TLM and the YFM, to show that, eliminating the detrimental effect of the contact resistance, can almost double the carrier field-effect mobility.

## ORCID iDs

Antonio Di Bartolomeo  <https://orcid.org/0000-0002-3629-726X>

## References

- [1] Novoselov K S 2004 Electric field effect in atomically thin carbon films *Science* **306** 666–9
- [2] Novoselov K S, Geim A K, Morozov S V, Jiang D, Katsnelson M I, Grigorieva I V, Dubonos S V and Firsov A A 2005 Two-dimensional gas of massless dirac fermions in graphene *Nature* **438** 197–200
- [3] Geim A K and Novoselov K S 2007 The rise of graphene *Nature Mater* **6** 183–91
- [4] Xu M, Liang T, Shi M and Chen H 2013 Graphene-like two-dimensional materials *Chem. Rev.* **113** 3766–98
- [5] Carvalho A, Wang M, Zhu X, Rodin A S, Su H and Castro Neto A H 2016 Phosphorene: from theory to applications *Nat Rev Mater* **1** 16061
- [6] Urban F *et al* 2019 Gas dependent hysteresis in MoS<sub>2</sub> field effect transistors *2D Mater.* **6** 045049
- [7] Giubileo F, Grillo A, Passacantando M, Urban F, Iemmo L, Luongo G, Pelella A, Loveridge M, Lozzi L and Di Bartolomeo A 2019 Field emission characterization of MoS<sub>2</sub> nanoflowers *Nanomaterials* **9** 717
- [8] Ahn J-H, Parkin W M, Naylor C H, Johnson A T C and Drndić M 2017 Ambient effects on electrical characteristics of CVD-grown monolayer MoS<sub>2</sub> field-effect transistors *Sci. Rep.* **7** 4075
- [9] Grillo A, Giubileo F, Iemmo L, Luongo G, Urban F and Di Bartolomeo A 2019 Space charge limited current and photoconductive effect in few-layer MoS<sub>2</sub> *J. Phys.: Conf. Ser* **1226012013**
- [10] Rai A, Valsaraj A, Movva H C P, Roy A, Tutuc E, Register L F and Banerjee S K 2015 Interfacial-oxygen-vacancy mediated doping of MoS<sub>2</sub> by high- $\kappa$  dielectrics *Proc. of the 2015 73rd Annual Device Research Conf. (DRC)* pp 189–90
- [11] Di Bartolomeo A *et al* Asymmetric Schottky contacts in bilayer MoS<sub>2</sub> field effect transistors *Adv. Funct. Mater.* **28** 1800657
- [12] Das S, Chen H-Y, Penumatcha A V and Appenzeller J 2013 High performance multilayer MoS<sub>2</sub> transistors with scandium contacts *Nano Lett.* **13** 100–5
- [13] Urban F, Passacantando M, Giubileo F, Iemmo L and Di Bartolomeo A 2018 Transport and field emission properties of MoS<sub>2</sub> bilayers *Nanomaterials* **8** 151
- [14] Iemmo L, Urban F, Giubileo F, Passacantando M and Di Bartolomeo A 2020 Nanotip contacts for electric transport and field emission characterization of ultrathin MoS<sub>2</sub> flakes *Nanomaterials* **10** 106
- [15] Feng C, Xiang J, Liu P and Xiang B 2017 The growth study of bilayer and monolayer WSe<sub>2</sub> *Mater. Res. Express* **4** 095703
- [16] Urban F, Martucciello N, Peters L, McEvoy N and Di Bartolomeo A 2018 Environmental effects on the electrical characteristics of back-gated WSe<sub>2</sub> field-effect transistors *Nanomaterials* **8** 901
- [17] Di Bartolomeo A, Urban F, Passacantando M, McEvoy N, Peters L, Iemmo L, Luongo G, Romeo F and Giubileo F 2019 A WSe<sub>2</sub> vertical field emission transistor *Nanoscale* **11** 1538
- [18] Di Bartolomeo A, Pelella A, Liu X, Miao F, Passacantando M, Giubileo F, Grillo A, Iemmo L, Urban F and Liang S-J 2019 Pressure-tunable ambipolar conduction and hysteresis in thin palladium diselenide field effect transistors *Adv. Funct. Mater.* **29** 1902483
- [19] Long C, Liang Y, Jin H, Huang B and Dai Y 2019 PdSe<sub>2</sub>: flexible two-dimensional transition metal dichalcogenides monolayer for water splitting photocatalyst with extremely low recombination rate *ACS Appl. Energy Mater.* **2** 513–20
- [20] Yim C, Passi V, Lemme M C, Duesberg G S, Ó Coileáin C, Pallecchi E, Fadil D and McEvoy N 2018 Electrical devices from top-down structured platinum diselenide films *Npj 2D Mater Appl* **2** 5
- [21] Ansari L *et al* 2019 Quantum confinement-induced semimetal-to-semiconductor evolution in large-area ultra-thin PtSe<sub>2</sub> films grown at 400 °C *Npj 2D Mater Appl* **3** 33
- [22] Schwierz F 2010 Graphene transistors *Nat. Nanotechnol.* **5** 487
- [23] Meric I, Dean C R, Young A F, Baklitskaya N, Tremblay N J, Nuckolls C, Kim P and Shepard K L 2011 Channel length scaling in graphene field-effect transistors studied with pulsed current–voltage measurements *Nano Lett.* **11** 1093–7
- [24] Castro Neto A H, Guinea F, Peres N M R, Novoselov K S and Geim A K 2009 The electronic properties of graphene *Rev. Mod. Phys.* **81** 109–62
- [25] Ghosh S, Calizo I, Teweldebrhan D, Pokatilov E P, Nika D L, Balandin A A, Bao W, Miao F and Lau C N 2008 Extremely high thermal conductivity of graphene: prospects for thermal management applications in nanoelectronic circuits *Appl. Phys. Lett.* **92** 151911
- [26] Nagashio K, Nishimura T, Kita K and Toriumi A 2009 Mobility variations in mono- and multi-layer graphene films *Appl. Phys. Express* **2** 025003

- [27] Wolf E L 2014 *Graphene: a new paradigm in condensed matter and device physics* 1st edn (Oxford: Oxford University Press) (<https://doi.org/10.1093/acprof:oso/9780199645862.001.0001>)
- [28] Yi M and Shen Z 2015 A review on mechanical exfoliation for the scalable production of graphene *J. Mater. Chem. A* **3** 11700–15
- [29] Gayathri S, Jayabal P, Kottaisamy M and Ramakrishnan V 2014 Synthesis of few layer graphene by direct exfoliation of graphite and a Raman spectroscopic study *AIP Adv.* **4** 027116
- [30] Huang H, Chen S, Wee A T S and Chen W 2014 Epitaxial growth of graphene on silicon carbide (SiC) *Graphene* (Amsterdam: Elsevier) pp 3–26
- [31] Wang C, Vinodgopal K and Dai G-P 2019 Large-area synthesis and growth mechanism of graphene by chemical vapor deposition *Chemical Vapor Deposition for Nanotechnology* ed P Mandracci (Rijeka: IntechOpen) (<https://doi.org/10.5772/intechopen.79959>)
- [32] Juang Z-Y, Wu C-Y, Lu A-Y, Su C-Y, Leou K-C, Chen F-R and Tsai C-H 2010 Graphene synthesis by chemical vapor deposition and transfer by a roll-to-roll process *Carbon* **48** 3169–74
- [33] Luongo G, Bartolomeo A D, Giubileo F, Chavarin C A and Wenger C 2018 Electronic properties of graphene/p-silicon Schottky junction *J. Phys. D: Appl. Phys.* **51** 255305
- [34] Luongo G, Giubileo F, Iemmo L and Di Bartolomeo A 2018 The role of the substrate in graphene/silicon photodiodes *J. Phys.: Conf. Ser.* **956** 012019
- [35] Feng X, Zhao X, Yang L, Li M, Qie F, Guo J, Zhang Y, Li T, Yuan W and Yan Y 2018 All carbon materials pn diode *Nat. Commun.* **9** 3750
- [36] Luongo G, Grillo A, Giubileo F, Iemmo L, Lukosius M, Alvarado Chavarin C, Wenger C and Di Bartolomeo A 2019 Graphene Schottky junction on pillar patterned silicon substrate *Nanomaterials* **9** 659
- [37] Lemme M C 2009 Current status of graphene transistors *SSP* **156–158** 499–509
- [38] Yang H, Heo J, Park S, Song H J, Seo D H, Byun K-E, Kim P, Yoo I, Chung H-J and Kim K 2012 Graphene barristor, a triode device with a gate-controlled schottky barrier *Science* **336** 1140–3
- [39] Vaziri S, Lupina G, Henkel C, Smith A D, Östling M, Dabrowski J, Lippert G, Mehr W and Lemme M C 2013 A graphene-based hot electron transistor *Nano Lett.* **13** 1435–9
- [40] Iemmo L, Di Bartolomeo A, Giubileo F, Luongo G, Passacantando M, Niu G, Hatami F, Skibitzki O and Schroeder T 2017 Graphene enhanced field emission from InP nanocrystals *Nanotechnology* **28** 495705
- [41] Giubileo F, Di Bartolomeo A, Iemmo L, Luongo G and Urban F 2018 Field emission from carbon nanostructures *Applied Sciences* **8** 526
- [42] Kim H-Y, Lee K, McEvoy N, Yim C and Duesberg G S 2013 Chemically modulated graphene diodes *Nano Lett.* **13** 2182–8
- [43] Shivananju B N, Yu W, Liu Y, Zhang Y, Lin B, Li S and Bao Q 2017 The roadmap of graphene-based optical biochemical sensors *Adv. Funct. Mater.* **27** 1603918
- [44] Di Bartolomeo A, Giubileo F, Luongo G, Iemmo L, Martucciello N, Niu G, Fraschke M, Skibitzki O, Schroeder T and Lupina G 2016 Tunable Schottky barrier and high responsivity in graphene/Si-nanotip optoelectronic device *2D Mater.* **4** 015024
- [45] Xia F, Mueller T, Lin Y, Valdes-Garcia A and Avouris P 2009 Ultrafast graphene photodetector *Nat. Nanotechnol.* **4** 839–43
- [46] Riazimehr S, Bablich A, Schneider D, Kataria S, Passi V, Yim C, Duesberg G S and Lemme M C 2016 Spectral sensitivity of graphene/silicon heterojunction photodetectors *Solid-State Electronics* **115** 207–12
- [47] Luongo G, Giubileo F, Genovese L, Iemmo L, Martucciello N and Di Bartolomeo A 2017 I-V and C-V Characterization of a high-responsivity graphene/silicon photodiode with embedded MOS capacitor *Nanomaterials* **7** 158
- [48] Riazimehr S, Kataria S, Bornemann R, Haring Bolívar P, Ruiz F J G, Engström O, Godoy A and Lemme M C 2017 High photocurrent in gated graphene-silicon hybrid photodiodes *ACS Photonics* **4** 1506–14
- [49] Di Bartolomeo A, Luongo G, Giubileo F, Funicello N, Niu G, Schroeder T, Lisker M and Lupina G 2017 Hybrid graphene/silicon Schottky photodiode with intrinsic gating effect *2D Mater.* **4** 025075
- [50] Luo F, Zhu M, Tan Y, Sun H, Luo W, Peng G, Zhu Z, Zhang X-A and Qin S 2018 High responsivity graphene photodetectors from visible to near-infrared by photogating effect *AIP Adv.* **8** 115106
- [51] Mahmoudi T, Wang Y and Hahn Y-B 2018 Graphene and its derivatives for solar cells application *Nano Energy* **47** 51–65
- [52] Mina A N, Awadallah A A, Phillips A H and Ahmed R R 2012 Simulation of the band structure of graphene and carbon nanotube *J. Phys.: Conf. Ser.* **343** 012076
- [53] Yankowitz M, Jung J, Laksono E, Leconte N, Chittari B L, Watanabe K, Taniguchi T, Adam S, Graf D and Dean C R 2018 Dynamic band-structure tuning of graphene moiré superlattices with pressure *Nature* **557** 404–8
- [54] Nag A, Kumar J and Sastri O S K S 2015 Electronic properties of graphene and effect of doping on the same. *AIP Conf. Proc.* **1661** 080021
- [55] Sahu S and Rout G C 2017 Band gap opening in graphene: a short theoretical study *Int Nano Lett* **7** 81–9
- [56] Schwierz F 2013 Graphene transistors: status, prospects, and problems *Proc. IEEE* **101** 1567–84
- [57] Lisker M, Lukosius M, Kitzmann J, Fraschke M, Wolansky D, Schulze S, Lupina G and Mai A 2018 Contacting graphene in a 200 nm wafer silicon technology environment *Solid-State Electronics* **144** 17–21
- [58] Gahoi A, Wagner S, Bablich A, Kataria S, Passi V and Lemme M C 2016 Contact resistance study of various metal electrodes with CVD graphene *Solid-State Electronics* **125** 234–9
- [59] Di Bartolomeo A, Giubileo F, Iemmo L, Romeo F, Santandrea S and Gambardella U 2013 Transfer characteristics and contact resistance in Ni- and Ti-contacted graphene-based field-effect transistors *J. Phys. Condens. Matter* **25** 155303
- [60] Nagashio K, Nishimura T, Kita K and Toriumi A 2010 Systematic investigation of the intrinsic channel properties and contact resistance of monolayer and multilayer graphene field-effect transistor *Jpn. J. Appl. Phys.* **49** 051304
- [61] Xia F, Perebeinos V, Lin Y, Wu Y and Avouris P 2011 The origins and limits of metal-graphene junction resistance *Nature Nanotech* **6** 179–84
- [62] Watanabe E, Conwill A, Tsuya D and Koide Y 2012 Low contact resistance metals for graphene based devices *Diam. Relat. Mater.* **24** 171–4
- [63] Smith J T, Franklin A D, Farmer D B and Dimitrakopoulos C D 2013 Reducing contact resistance in graphene devices through contact area patterning *ACS Nano* **7** 3661–7
- [64] Min Song S, Yong Kim T, Jae Sul O, Cheol Shin W and Jin Cho B 2014 Improvement of graphene-metal contact resistance by introducing edge contacts at graphene under metal *Appl. Phys. Lett.* **104** 183506
- [65] Park H-Y et al 2016 Extremely low contact resistance on graphene through n-type doping and edge contact design *Adv. Mater.* **28** 864–70
- [66] Wang L et al 2013 One-dimensional electrical contact to a two-dimensional material *Science* **342** 614–7
- [67] Anzi L et al 2018 Ultra-low contact resistance in graphene devices at the Dirac point *2D Mater.* **5** 025014

- [68] Venugopal A, Colombo L and Vogel E M 2010 Contact resistance in few and multilayer graphene devices *Appl. Phys. Lett.* **96** 013512
- [69] Song S M 2013 **조병진** Contact resistance in graphene channel transistors *Carbon Letters* **14** 162–70
- [70] Gahoi A, Kataria S and Lemme M C 2017 Temperature dependence of contact resistance for gold-graphene contacts *Proc. of the 2017 47th European Solid-State Device Research Conf. (ESSDERC); IEEE: Leuven, Belgium* pp 110–3
- [71] Zhu M, Wu J, Du Z, Tsang S and Teo E H T 2018 Gate voltage and temperature dependent Ti-graphene junction resistance toward straightforward p-n junction formation *J. Appl. Phys.* **124** 215302
- [72] Zhong H, Zhang Z, Chen B, Xu H, Yu D, Huang L and Peng L 2015 Realization of low contact resistance close to theoretical limit in graphene transistors *Nano Res.* **8** 1669–79
- [73] Anteroinen J, Kim W, Stadius K, Riikonen J, Lipsanen H and Ryyanen J 2012 Extraction of graphene-titanium contact resistances using transfer length measurement and a curve-fit method
- [74] Schroder D K 2006 *Semiconductor Material and Device Characterization* (New York: Wiley) pp 156
- [75] Russo S, Craciun M F, Yamamoto M, Morpurgo A F and Tarucha S 2010 Contact resistance in graphene-based devices *Physica E* **42** 677–9
- [76] Giannazzo F, Fisichella G, Piazza A, Di Franco S, Greco G, Agnello S and Roccaforte F 2017 Impact of contact resistance on the electrical properties of MoS<sub>2</sub> transistors at practical operating temperatures *Beilstein J. Nanotechnol.* **8** 254–63
- [77] Wang S, Mao D, Jin Z, Peng S, Zhang D, Shi J and Wang X 2015 A more reliable measurement method for metal/graphene contact resistance *Nanotechnology* **26** 405706
- [78] Ghibaudo G 1988 New method for the extraction of MOSFET parameters *Electron. Lett.* **24** 543
- [79] Henry J B, Raffay Q, Cros A and Ghibaudo G 2016 New Y-function based MOSFET parameter extraction method from weak to strong inversion range *Solid-State Electronics* **123** 84–8
- [80] Lai S, Cosseddu P and Bonfiglio A 2017 A method for direct contact resistance evaluation in low voltage coplanar organic field-effect transistors *Appl. Phys. Lett.* **110** 153304
- [81] Lukosius M et al 2016 Metal-free CVD graphene synthesis on 200 mm Ge/Si(001) substrates *ACS Appl. Mater. Interfaces* **8** 33786–93
- [82] Giubileo F and Di Bartolomeo A 2017 The role of contact resistance in graphene field-effect devices *Prog. Surf. Sci.* **92** 143–75
- [83] Diouf C, Cros A, Monfray S, Mitard J, Rosa J, Gloria D and Ghibaudo G 2013 ‘Y function’ method applied to saturation regime: Apparent saturation mobility and saturation velocity extraction *Solid-State Electronics* **85** 12–4
- [84] Bartolomeo A D, Giubileo F, Romeo F, Sabatino P, Carapella G, Lemmo L, Schroeder T and Lupina G 2015 Graphene field effect transistors with niobium contacts and asymmetric transfer characteristics *Nanotechnology* **26** 475202
- [85] Farmer D B, Golizadeh-Mojarad R, Perebeinos V, Lin Y-M, Tulevski G S, Tsang J C and Avouris P 2009 Chemical doping and electron–hole conduction asymmetry in graphene devices *Nano Lett.* **9** 388–92
- [86] Barraza-Lopez S, Vanević M, Kindermann M and Chou M Y 2010 Effects of metallic contacts on electron transport through graphene *Phys. Rev. Lett.* **104** 076807
- [87] Toral-Lopez A, Marin E G, Pasadas F, Gonzalez-Medina J M, Ruiz F G, Jiménez D and Godoy A 2019 GFET asymmetric transfer response analysis through access region resistances *Nanomaterials* **9** 1027
- [88] Bartolomeo A D, Giubileo F, Santandrea S, Romeo F, Citro R, Schroeder T and Lupina G 2011 Charge transfer and partial pinning at the contacts as the origin of a double dip in the transfer characteristics of graphene-based field-effect transistors *Nanotechnology* **22** 275702
- [89] Wei J, Liang B, Cao Q, Ren H, Zheng Y and Ye X 2020 Understanding asymmetric transfer characteristics and hysteresis behaviors in graphene devices under different chemical atmospheres *Carbon* **156** 67–76
- [90] Di Bartolomeo A, Yang Y, Rinzan M B M, Boyd A K and Barbara P 2010 Record endurance for single-walled carbon nanotube-based memory cell *Nanoscale Res. Lett.* **5** 1852
- [91] Di Bartolomeo A, Santandrea S, Giubileo F, Romeo F, Petrosino M, Citro R, Barbara P, Lupina G, Schroeder T and Rubino A 2013 Effect of back-gate on contact resistance and on channel conductance in graphene-based field-effect transistors *Diam. Relat. Mater.* **38** 19–23
- [92] Mogera U, Walia S, Bannur B, Gedda M and Kulkarni G U 2017 Intrinsic nature of graphene revealed in temperature-dependent transport of twisted multilayer graphene *J. Phys. Chem. C* **121** 13938–43
- [93] Mayorov A S, Elias D C, Mukhin I S, Morozov S V, Ponomarenko L A, Novoselov K S, Geim A K and Gorbachev R V 2012 How close can one approach the dirac point in graphene experimentally? *Nano Lett.* **12** 4629–34
- [94] Das Sarma S and Hwang E H 2013 Density-dependent electrical conductivity in suspended graphene: approaching the dirac point in transport *Phys. Rev. B* **87** 035415
- [95] Bolotin K I, Sikes K J, Hone J, Stormer H L and Kim P 2008 Temperature-dependent transport in suspended graphene *Phys. Rev. Lett.* **101** 096802
- [96] Lundstrom M and Jeong C 2013 Near-equilibrium transport: fundamentals and applications *Lessons from Nanoscience* (Singapore: World Scientific)
- [97] Chen Z and Appenzeller J 2008 Mobility extraction and quantum capacitance impact in high performance graphene field-effect transistor devices *Proc. of the 2008 IEEE Int. Electron Devices Meeting; IEEE: San Francisco, CA, USA* pp 1–4
- [98] Chen J-H, Jang C, Xiao S, Ishigami M and Fuhrer M S 2008 Intrinsic and extrinsic performance limits of graphene devices on SiO<sub>2</sub> *Nat. Nanotechnol.* **3** 206
- [99] Zhu W, Perebeinos V, Freitag M and Avouris P 2009 Carrier scattering, mobilities, and electrostatic potential in monolayer, bilayer, and trilayer graphene *Phys. Rev. B* **80** 235402
- [100] Dorgan V E, Bae M-H and Pop E 2010 Mobility and saturation velocity in graphene on SiO<sub>2</sub> *Appl. Phys. Lett.* **97** 082112